Contribution No. 2177 from the Central Research Department, Experimental Station, E. I. du Pont de Nemours and Company

New Ternary Oxides of Pentavalent and Hexavalent Rhenium of the Type $AReO_4$ or A_2ReO_6

A. W. SLEIGHT

Received August 26, 1974 AIC40613Z

Compounds of the type $AReO_4$ where A is Mg, Mn, Fe, Co, Ni, Zn, Al, and Ga have been prepared. Most have structures related to that of rutile, but the wolframite structure is observed for A = Mg, Mn, and Zn. $MnReO_4$ exhibits anisotropic electrical resistivity. Cr_2ReO_6 was prepared in the trirutile structure, and Fe_2ReO_6 has the tri-α-PbO_2 structure. All of these new oxides of rhenium appear to require high pressure for their synthesis. These compounds represent the first cases in all of these structure types where both cations have open d shells.

Introduction

Rhenium oxides of the type $AReO_4$ are well known where the A cation is univalent and Re is in its group oxidation state of VII. However, $AReO_4$ compounds have not been reported where Re is in an oxidation state of less than VII. Compounds of the type A_2ReO_6 have not been reported for any oxidation state of Re. If A were a first-row transition metal cation, an interesting combination of localized 3d electrons and delocalized 5d electrons might result. Thus, attempts were made to synthesize compounds of these types.

Experimental Section

Rhenium trioxide was obtained from ROC/RIC. All other reactants were reagent grade or better. Syntheses were carried out in a tetrahedral anvil previously described.[1] The conditions were generally 58 kbars at 1200–1300° for 1–4 hr using platinum containers. Reactant ratios are given in Table I.

X-Ray powder patterns were recorded at 25° using a Hägg–Guinier camera with $CuK\alpha_1$ radiation and an internal standard of high-purity KCl (a = 6.2931 Å). Indexed powder patterns have been submitted to ASTM. Electrical data were obtained by the four-probe method using indium-solder contacts.

Results

The new $AReO_4$ and A_2ReO_6 phases prepared are listed in Table I. These compounds are all black or dark violet. The pressure required for the syntheses of these phases was not determined, but 30 kbars was adequate to prepare $MnReO_4$. Synthesis attempts at 3 kbars were unsuccessful; thus, substantial pressure is apparently necessary. Therefore, these compounds all appear to be metastable, but they exist for years at ambient conditions without noticeable decomposition. Chemical analyses were not attempted in view of the very small sample size. However, closed containers were used for syntheses, and the products were single phase. Thus, the compositions of the products are determined by the reactants.

$MgReO_4$, $MnReO_4$, and $ZnReO_4$. These compounds apparently have the wolframite structure. The cell dimensions are given in Table I. The intensities of reflections from powder patterns were compared to those from analogous tungstates, and they were qualitatively the same. Single-crystal X-ray photographs of $MnReO_4$ were consistent with the wolframite structure.

Crystals of $MnReO_4$ large enough for anisotropic resistivity measurements were obtained. At room temperature the resistivity parallel to the c axis was 0.39 ohm cm, and perpendicular to this axis the resistivity was 3.1 ohm cm. The activation energy was 0.4 eV in both directions. The magnetic susceptibility of $MnReO_4$ was investigated from 78 to 298°K. The room-temperature molar susceptibility was 23×10^3. This smoothly decreased to 17.5×10^3 at 210°K and then smoothly increased to 19×10^3 at 78°K.

$AlReO_4$, $GaReO_4$, and $FeReO_4$. These phases presumably have the rutile structure with a statistical distribution of the cations. A single crystal of $FeReO_4$ showed a room temperature electrical resistivity of 8×10^{-4} ohm cm which decreased slightly on cooling. Magnetic measurements indicated antiferromagnetism with a Neel temperature of 194°K.

$NiReO_4$ and $CoReO_4$. These phases also appear to have structures related to that of rutile. However, they are definitely not tetragonal. A simple orthorhombic distortion was indicated for $NiReO_4$ (Table I). A different type of orthorhombic distortion was indicated for $CoReO_4$. This is a C-centered orthorhombic cell where a and b are larger by a factor of $2^{1/2}$. This cell for $CoReO_4$ was confirmed by single-crystal X-ray studies.

Cr_2ReO_6 and Fe_2ReO_6. The powder pattern of Cr_2ReO_6 was readily indexed on the basis of the trirutile structure. A comparison of intensities with those from Cr_2WO_6 confirmed that Cr_2ReO_6 and Cr_2WO_6 are essentially isostructural. Fe_2ReO_6 is isostructural with Fe_2WO_6 which has been described[2] as having a tri-α-PbO_2 structure.

Table I. Synthesis and Crystallographic Data[a]

Compd	a, Å	b, Å	c, Å	β, deg	Reactants
$MgReO_4$	4.690	5.573	5.066	92.03	MgO–ReO_3
$MnReO_4$	4.802	5.630	5.076	92.73	$3MnO_2$–$2ReO_3$–Re
$ZnReO_4$	4.695	5.605	5.026	91.27	ZnO–ReO_3
$AlReO_4$	4.636		2.803		$3Al_2O_3$–$5ReO_3$–Re
$GaReO_4$	4.692		2.850		$3Ga_2O_3$–$5ReO_3$–Re
$FeReO_4$	4.668		2.927		$3Fe_2O_3$–$5ReO_3$–Re
$NiReO_4$	4.625	4.678	2.893		NiO–ReO_3
$CoReO_4$	6.503	6.732	2.881		Co_3O_4–Co–$4ReO_3$
Cr_2ReO_6	4.551		8.907		Cr_2O_3–ReO_3
Fe_2ReO_6	4.541	16.629	4.974		Fe_2O_3–ReO_3

[a] Errors in cell edges are estimated to be ±0.05%.

Discussion

All of the new compounds reported here have structures based on hexagonal close-packed oxygen layers with all cations in octahedral sites. Since the oxygen-to-total metal ratio is 2 in all cases, half of the octahedral sites are occupied. Two fundamentally different ways of filling these sites are relevant to this discussion. In the rutile structure, there are linear chains of edge-shared octahedra. The α-PbO_2 structure also has chains of edge-shared octahedra, but here the chains are zigzagged. Substitutions of the type $A^{III}M^{V}O_4$ in the rutile structure (*e.g.*, $FeTaO_4$) have never led to a long-range ordering of the cations.[3] (Actually, there may be a very high degree of order along a chain; but due to the particular geometry, there is essentially no electrostatic incentive for such chains to order with respect to one another. Thus, there is no long-range order in three dimensions). Substitutions of the type $A^{III}M^{V}O_4$ are not known in the rutile structure. However, substitutions of the types $A^{II}M^{V}{}_2O_6$ and $A^{III}{}_2M^{VI}O_6$ in the rutile structure (*e.g.*, $MgTa_2O_6$ and Cr_2WO_6) are accompanied by long-range ordering of A and M in three dimensions.[4,5] The resulting structure is referred to as the trirutile structure. Ordering of cations in the α-PbO_2 structure can occur for either the AMO_4

or the A_2MO_6 compositions. The structure of the ordered α-PbO_2 arrangement is known as the wolframite structure for the AMO_4 composition. There are two different possibilities for the A_2MO_6 (or AM_2O_6) composition. These are referred to as the tri-α-PbO_2 or the columbite structure.[2,3]

The oxidation state of the A cation is definite in $Mg^{II}ReO_4$, $Zn^{II}ReO_4$, $Al^{III}ReO_4$, and $Ga^{III}ReO_4$. Thus, it is certain that $AReO_4$ compounds have been prepared where rhenium is formally pentavalent and where it is formally hexavalent. The wolframite structure is found for the definite $A^{II}Re^{VI}O_4$ situation, and the statistical rutile structure is found for the definite $A^{III}Re^{V}O_4$ combination.

The oxidation states in $FeReO_4$ might be Fe^{II}–Re^{VI} or Fe^{III}–Re^{V}. This is a particularly interesting problem since the oxidation states in Ba_2FeMoO_6 are Fe^{III}–Mo^{V},[6,7] while in all three forms of $FeMoO_4$ the Fe^{II}–Mo^{VI} combination prevails.[8] In Ba_2FeReO_6 the oxidation states are Fe^{III}–Re^{V}, but it is proposed that this combination is nearly degenerate with the Fe^{II}–Re^{VI} situation.[9] Thus, the oxidation states in $FeReO_4$ could not be predicted. The fact that $FeReO_4$ is isostructural with $Al^{III}Re^{V}O_4$ and $Ga^{III}Re^{V}O_4$ rather than $Mg^{II}Re^{VI}O_4$ and $Zn^{II}Re^{VI}O_4$ strongly suggests that the oxidation states are Fe^{III}–Re^{V} in $FeReO_4$. This is an especially strong argument since *no* $A^{II}M^{VI}O_4$ compounds are known to have the rutile structure. A $Fe^{III}Re^{V}O_4$ combination is further supported by the cell volume of $FeReO_4$ relative to the cell volumes of $AlReO_4$ and $GaReO_4$. The volume for $GaReO_4$ is slightly less than that of $FeReO_4$ which is expected if the iron is trivalent. A $Fe^{II}Re^{VI}O_4$ combination would be expected to give a significantly larger cell volume.

The oxidation states in $CoReO_4$ and $NiReO_4$ are less certain. In Ba_2CoReO_6 and Ba_2NiReO_6, the oxidation states are A^{II}–Re^{VI},[9] and there is no suggestion of valence degeneracy as indicated for Ba_2FeReO_6. Thus, an A^{II}–Re^{VI} combination might be expected for both $NiReO_4$ and $CoReO_4$. However, it then becomes somewhat surprising that these compounds do not have the wolframite structure. The answer may be that $CoReO_4$ and $NiReO_4$ are $A^{III}Re^{V}O_4$ at high pressure where they adopt a rutile-type structure. High pressure would tend to favor A^{III}–Re^{V} over A^{II}–Re^{VI} since the former would have a higher density. This is true because whereas Re^{V} is slightly larger than Re^{VI}, A^{II} is considerably larger than A^{III}. On release of the pressure, the valence situation might go from A^{III}–Re^{V} to A^{II}–Re^{VI}. However, the disorder and delocalization in $NiReO_4$ and $CoReO_4$ may lead to a situation where neither A^{II}–Re^{VI} nor A^{III}–Re^{V} applies.

The cell dimensions for all $A^{II}M^{VI}O_4$ compounds with the wolframite structure are plotted in Figure 1 as a function of the radius[10] of A^{II}. All compounds with this structure show essentially the same behavior with respect to the *a* dimension. However, $MgTeO_4$[11] and the $AReO_4$ compounds show a larger *c* and a smaller *b* dimension than the analogous molybdates and tungstates. The wolframite structure consists of edge-shared octahedra chains which are parallel to the *c* axis. Thus, for $MgTeO_4$ and the $AReO_4$ compounds, the cation–cation distances within the chains are probably longer but the chains are closer together relative to the analogous tungstates and molybdates. However, this is not a firm conclusion since the positional parameters in these phases have not been refined.

In tungstates and molybdates with the wolframite structure, there is considerable distortion of the octahedra surrounding Mo and W. This distortion is almost certainly related to multiple-bond formation between Mo or W and oxygen using the empty d orbitals of Mo or W. Such bonding is impossible for Te with its closed d shell. Such bonding is also unlikely for Re^{VI}, especially if its antibonding 5d electron is delocalized. Thus, the octahedra around Re^{VI} and Te^{VI} are almost certain to be more regular, and this is probably the primary reason for their different behavior in Figure 1. The points for $MnReO_4$ in Figure 1 offer good support for a Mn^{II}–Re^{VI} valence combination.

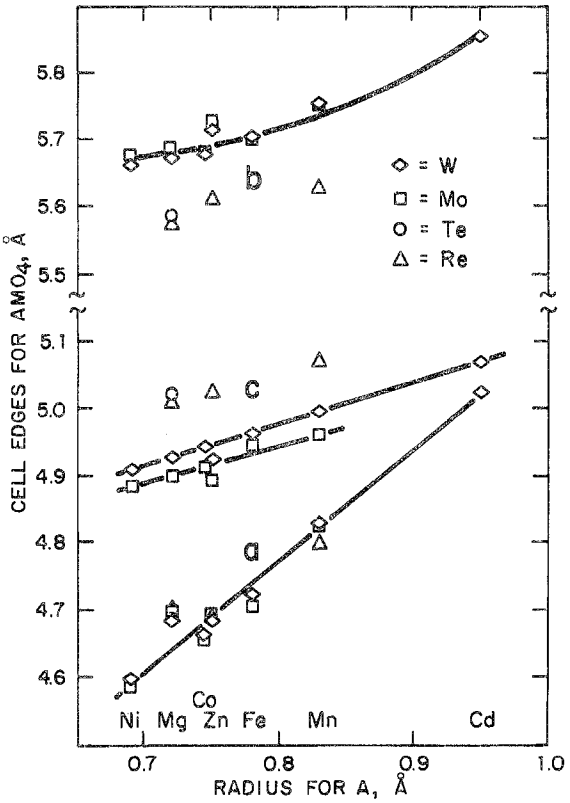

Figure 1. Cell edges *vs.* radius of A for AMO_4 compounds with the wolframite structure.

$MnReO_4$ is the first compound to be prepared with the wolframite structure where both cations have partially filled d shells. The d electrons of Re^{VI} should be very delocalized relative to those of Mn^{II}. Since there are infinite Re–O–Re–O and Re–Re–Re linkages along the *c* axis but not perpendicular to it, anisotropic electrical resistivity might well be expected. In fact, metallic behavior might be expected along *c* with semiconducting behavior perpendicular to *c*. However, defects will generally preclude one-dimensional metals. Thus, it may be that the Re edge-shared octahedra do result in one-dimensional metallic behavior over a finite distance. However, an activation energy is required for a conduction electron to pass through a defect in a chain, and an activation energy is also required for an electron to pass from one chain to another. In fact, the easiest path for a conduction electron encountering a defect might be to jump to a neighboring chain. Thus, it is entirely reasonable that the activation energy in the two directions is the same but that the conductivity is somewhat better along the *c* axis.

Acknowledgment. The operation of the tetrahedral anvil was supervised by C. L. Hoover. The electrical resistivity data were provided by J. L. Gillson, and the magnetic measurements were carried out by J. F. Weiher. X-Ray data were obtained with the assistance of C. M. Foris.

Registry No. $MgReO_4$, 53849-95-9; $MnReO_4$, 53849-96-0; $ZnReO_4$, 53849-97-1; $AlReO_4$, 53906-75-5; $GaReO_4$, 53906-76-6; $FeReO_4$, 53906-77-7; $NiReO_4$, 53906-78-8; $CoReO_4$, 53906-79-9; Cr_2ReO_6, 53849-98-2; Fe_2ReO_6, 53849-99-3.

References and Notes

(1) A. W. Sleight and T. A. Bither, *Inorg. Chem.*, **8**, 566 (1969).
(2) J. Galy and J. Senegas, *C. R. Acad. Sci., Ser. C*, **275**, 665 (1972).
(3) K. Brandt, *Ark. Kemi, Mineral. Geol.*, **17A**, 1 (1943).
(4) A. Bystrom, B. Hok, and B. Mason, *Ark. Kemi, Mineral. Geol.*, **15B**, 1 (1941).
(5) G. Bayer, *J. Amer. Ceram. Soc.*, **43**, 495 (1960).

(6) T. Nakagawa, *J. Phys. Soc. Jap.*, **24**, 806 (1968).
(7) S. Nakayama, T. Nakagawa, and S. Nomura, *J. Phys. Soc. Jap.*, **24**, 219 (1968).
(8) A. W. Sleight, B. L. Chamberland, and J. F. Weiher, *Inorg. Chem.*, **7**, 1093 (1968).
(9) A. W. Sleight and J. F. Weiher, *J. Phys. Chem. Solids*, **33**, 679 (1972).
(10) R. D. Shannon and C. T. Prewitt, *Acta Crystallogr., Sect. B*, **25**, 925 (1969).
(11) A. W. Sleight, C. M. Foris, and M. S. Licis, *Inorg. Chem.*, **11**, 1157 (1972).

Contribution from the Department of Chemistry, University of Michigan, Ann Arbor, Michigan 48104

Molecular Structures of P_2F_4 and $P_2(CF_3)_4$ by Gas-Phase Electron Diffraction[1]

H. L. HODGES, L. S. SU, and L. S. BARTELL*

Received August 2, 1974 AIC40531A

The principal structural parameters and uncertainties (2σ) for P_2F_4 are r_g(P–P) = 2.281 ± 0.006 Å, r_g(P–F) = 1.587 ± 0.003 Å, ∠PPF = 95.4 ± 0.3°, and ∠FPF = 99.1 ± 0.4°, and the rms libration about P–P is 16.7 ± 0.4°. Only trans conformers were observed. Gauche concentrations probably do not exceed 10% at room temperature. Corresponding values for $P_2(CF_3)_4$ were r_g(P–P) = 2.182 ± 0.016 Å, r_g(P–C) = 1.914 ± 0.004 Å, r_g(C–F) = 1.337 ± 0.002 Å, ∠CPC = 103.8 ± 0.8°, ∠PPC = 106.7 ± 0.7°, and ∠PCF = 110.4 ± 0.2°. Trans conformers predominated. Amplitudes of vibration were determined for both molecules. Structures of diphosphines provide no evidence for strong π delocalization across the P–P bond analogous to that found in aminophosphines. The longest P–P bond in diphosphines observed to date is that in P_2F_4, the molecule with the most electronegative ligands. The P–CF_3 bond is significantly longer than the P–CH_3 bond. Structural trends are in poor accord with VSEPR and semiempirical MO theories.

Introduction

The P–P bond in diphosphines has been the subject of many investigations. Several reviews have summarized the chemistry and structural features of compounds containing P–P linkages.[2-9] In diphosphines, the phosphorus atoms are joined by a σ bond, with each phosphorus bearing two substituent groups and an electron pair. It has been suggested that the unshared 3p electrons of one phosphorus are capable of overlap with the nominally unoccupied 3d orbitals of the second phosphorus in a $p\pi$–$d\pi$ interaction.[2,3,10-12] Such behavior, if significant, might correlate with substituent electronegativity and be discernible in trends of P–P bond lengths and molecular geometries in a series of diphosphines. Structural investigations have been reported for several diphosphines with substituents of modest electronegativity and for F_2PPH_2.[13] It seemed worthwhile to examine diphosphines with substituents of particularly high electronegativity on both phosphorus atoms. Therefore we initiated studies of P_2F_4 and $P_2(CF_3)_4$. In addition, a study of the Lewis base properties of diphosphines was carried out to indicate the availability of the lone pairs. Results are reported elsewhere.[14,15]

Experimental Section

The preparation of P_2F_4 is described elsewhere.[16] Purity was checked by infrared spectroscopy, the principal impurities being PF_3 and PF_2HO. The sample of $P_2(CF_3)_4$ was donated by Professor R. G. Cavell and used as received. Mass spectral analysis indicated a purity of at least 98%.

Electron diffraction patterns were recorded using an electron diffraction apparatus equipped with an r^3 rotating sector.[17] The samples were introduced through a nickel nozzle having a throat approximately 0.7 mm long and 0.29 mm in diameter and the nozzle lip was 0.47 mm from the center of the electron beam. All diffraction patterns of $P_2(CF_3)_4$ and patterns of P_2F_4 taken at the 21-cm camera distance were recorded on 4 × 5 in. Kodak process plates; those of P_2F_4 at the 11-cm camera distance were recorded on Kodak electron image plates. Kodak anti-fog solution was added to the developer in the case of the electron image plates. Experimental conditions for recording of the diffraction patterns are given in Table I.

For P_2F_4, two plates at the 21-cm camera distance and four plates at the 11-cm distance were selected for analysis. For $P_2(CF_3)_4$, five 21-cm and four 11-cm plates were analyzed. Photographic densities were measured with an automatic recording microphotometer with digital output.[18] Readings were taken at 1/8-mm intervals across the diameter of a spinning plate, and either the even or the odd set of 1/8-mm readings was used in the structure determination.

Table I. Experimental Conditions for Recording Diffraction Patterns

	P_2F_4		$P_2(CF_3)_4$	
Camera dist, cm	21.149	11.073	21.129	11.159
Reservoir temp, °C	Ambient	Ambient	−2	0
Vapor pressure, Torr	10–20	10–20	~20	~20
Exposure time, sec	4–5	5	2.2	5.5
Beam current, μA	0.32	0.37	0.46	0.46

Due to the extreme sensitivity of P_2F_4 to moisture, special attention was given to handling and monitoring for purity. The vacuum system was maintained at a pressure of 10^{-5} mm or better. All parts of the inlet system exposed to the atmosphere between runs were pumped down for a minimum of 4 hr. To avoid unnecessary decomposition in the liquid phase, the sample, stored in a Pyrex sample tube attached to a 300-ml Pyrex bulb, was maintained at −196° by a liquid nitrogen bath. Prior to a run, a small amount of P_2F_4 was expanded into the bulb connected to the nozzle by a stopcock. A gas-phase infrared cell was also attached to the bulb, and midway through a run a small amount of sample was expanded into the cell. The purity of the P_2F_4 was checked by infrared analysis at the end of a run, and if there was greater than approximately 5% impurity, the diffraction data were not used.

Analysis of Data

After recording the diffraction patterns, absorbances were measured by a digital microphotometer[18] and converted to exposures by the relation $E = A(1 + aA)$ where E is the exposure and A the corresponding absorbance and where a ranged from 0.05 to 0.10 for the various plates.

Exposures of the individual plates at a given camera distance were averaged and corrected for sector irregularities and extraneous scattering. Experimental intensities were leveled[19] using the elastic scattering factors of Strand and Bonham[20] and the inelastic scattering factors of Heisenberg[21] and Bewilogua.[22] For the 11-cm data of P_2F_4, an excessive rise in background intensity at large s necessitated a larger than normal extraneous scattering correction for the data at this camera distance to bring the background of the leveled intensity to a nearly horizontal line. The indices of resolution for P_2F_4 were 0.93 and 0.89 for the 21- and 11-cm camera distances, respectively, after correcting for extraneous scattering in the outer regions of the plates. The corresponding indices for $P_2(CF_3)_4$ were 1.06 and 1.01.

Reduced molecular intensities, $M(s)$, and radial distribution